



# Active contour configuration model for estimating the posterior ablative margin in image fusion of real-time ultrasound and 3D ultrasound or magnetic resonance images for radiofrequency ablation: an experimental study

ULTRA  
SONO  
GRAPHY

ORIGINAL ARTICLE

Junkyo Lee<sup>1,2</sup>, Min Woo Lee<sup>1,3</sup>, Dongil Choi<sup>1,3</sup>, Dong Ik Cha<sup>3</sup>, Sunyoung Lee<sup>3</sup>,  
Tae Wook Kang<sup>3</sup>, Jehoon Yang<sup>4</sup>, Jaemoon Jo<sup>5</sup>, Won-Chul Bang<sup>6</sup>, Jongsik Kim<sup>2</sup>,  
Dongkuk Shin<sup>2</sup>

<https://doi.org/10.14366/usg.17065>  
pISSN: 2288-5919 • eISSN: 2288-5943  
Ultrasonography 2018;37:337-344

\*Author affiliations appear at the end of this article.

**Purpose:** The purpose of this study was to evaluate the accuracy of an active contour model for estimating the posterior ablative margin in images obtained by the fusion of real-time ultrasonography (US) and 3-dimensional (3D) US or magnetic resonance (MR) images of an experimental tumor model for radiofrequency ablation.

**Methods:** Chickpeas (n=12) and bovine rump meat (n=12) were used as an experimental tumor model. Grayscale 3D US and T1-weighted MR images were pre-acquired for use as reference datasets. US and MR/3D US fusion was performed for one group (n=4), and US and 3D US fusion only (n=8) was performed for the other group. Half of the models in each group were completely ablated, while the other half were incompletely ablated. Hyperechoic ablation areas were extracted using an active contour model from real-time US images, and the posterior margin of the ablation zone was estimated from the anterior margin. After the experiments, the ablated pieces of bovine rump meat were cut along the electrode path and the cut planes were photographed. The US images with the estimated posterior margin were compared with the photographs and post-ablation MR images. The extracted contours of the ablation zones from 12 US fusion videos and post-ablation MR images were also matched.

**Results:** In the four models fused under real-time US with MR/3D US, compression from the transducer and the insertion of an electrode resulted in misregistration between the real-time US and MR images, making the estimation of the ablation zones less accurate than was achieved through fusion between real-time US and 3D US. Eight of the 12 post-ablation 3D US images were graded as good when compared with the sectioned specimens, and 10 of the 12 were graded as good in a comparison with nicotinamide adenine dinucleotide staining and histopathologic results.

**Conclusion:** Estimating the posterior ablative margin using an active contour model is a feasible way of predicting the ablation area, and US/3D US fusion was more accurate than US/MR fusion.

**Keywords:** Radiofrequency; Ablation techniques; Fusion imaging; Posterior; Shadowing; Ultrasonography

Received: November 4, 2017  
Revised: December 18, 2017  
Accepted: December 21, 2017

**Correspondence to:**  
Dongil Choi, MD, Department of  
Radiology, Samsung Medical Center,  
81 Irwon-ro, Gangnam-gu, Seoul  
06351, Korea

Tel. +82-2-3410-6415  
Fax. +82-2-3410-0084  
E-mail: [dichoi@skku.edu](mailto:dichoi@skku.edu)

This is an Open Access article distributed under the terms of the Creative Commons Attribution Non-Commercial License (<http://creativecommons.org/licenses/by-nc/3.0/>) which permits unrestricted non-commercial use, distribution, and reproduction in any medium, provided the original work is properly cited.

Copyright © 2018 Korean Society of  
Ultrasonography in Medicine (KSUM)



**How to cite this article:**  
Lee J, Lee MW, Choi D, Cha DI, Lee S, Kang TW, et al. Active contour configuration model for estimating the posterior ablative margin in image fusion of real-time ultrasound and 3D ultrasound or magnetic resonance images for radiofrequency ablation: an experimental study. Ultrasonography. 2018 Oct;37(4):337-344.

## Introduction

Radiofrequency (RF) ablation is widely used to treat hepatic tumors [1,2], as it is safe and effective [3,4]. The introduction of fusion imaging of real-time ultrasonography (US) and computed tomography (CT) or magnetic resonance (MR) images improved the accuracy of percutaneous RF ablation [5–7]. Among the various fusion imaging technologies, image fusion using electromagnetic position sensors is most commonly used in liver tumor ablation [8]. Fusion Imaging is useful for the RF ablation of very small tumors with poor lesion conspicuity, as reference data sets such as CT, MR, and 3-dimensional (3D) US images taken before the procedure increase lesion conspicuity [5–9]. When the tumor and inserted RF electrode are obscured by the hyperechoic zone created during the ablation, fused data sets provide useful information regarding whether the hyperechoic zone has covered the entire tumor or whether overlapping ablation is needed.

To facilitate successful RF ablation, planning for the placement of an electrode has been studied [10,11]. After ablation, technical success is usually evaluated using CT or MR imaging [12–15], and a second ablation session is performed if a viable tumor is identified on CT/MR images [14–16]. However, it is preferable to completely ablate the tumor during the first ablation session so that additional sessions can be avoided, as additional sessions extend patients'

hospital stay, increase the treatment costs, and increase discomfort for patients and operators. Therefore, it is important to evaluate the exact ablation zone during US-guided ablation in order to avoid re-treatment.

If the extent of the hyperechoic zone created from ablation is 5 mm larger than the tumor, the tumor can be expected to have been ablated sufficiently [12,17]. However, it is difficult to accurately identify the posterior ablative margin on US due to a posterior dirty shadow from the transient hyperechoic zone [18–20]. For this reason, we have developed an assessment tool that can evaluate the ablation zone in real time, which may make RF ablation more successful. The purpose of this preliminary study is to evaluate whether this assessment tool was effective in estimating the boundary of the ablation zone, including the posterior ablative margin.

## Materials and Methods

### Preparation of the Experimental Model

A pilot study was performed to find an appropriate experimental model for this study. Bovine rump meat was used to simulate the liver because it contains little adipose tissue, resulting in homogeneous US images. In the pilot study, chickpeas were determined to be the most suitable tumor substitute, as they had a

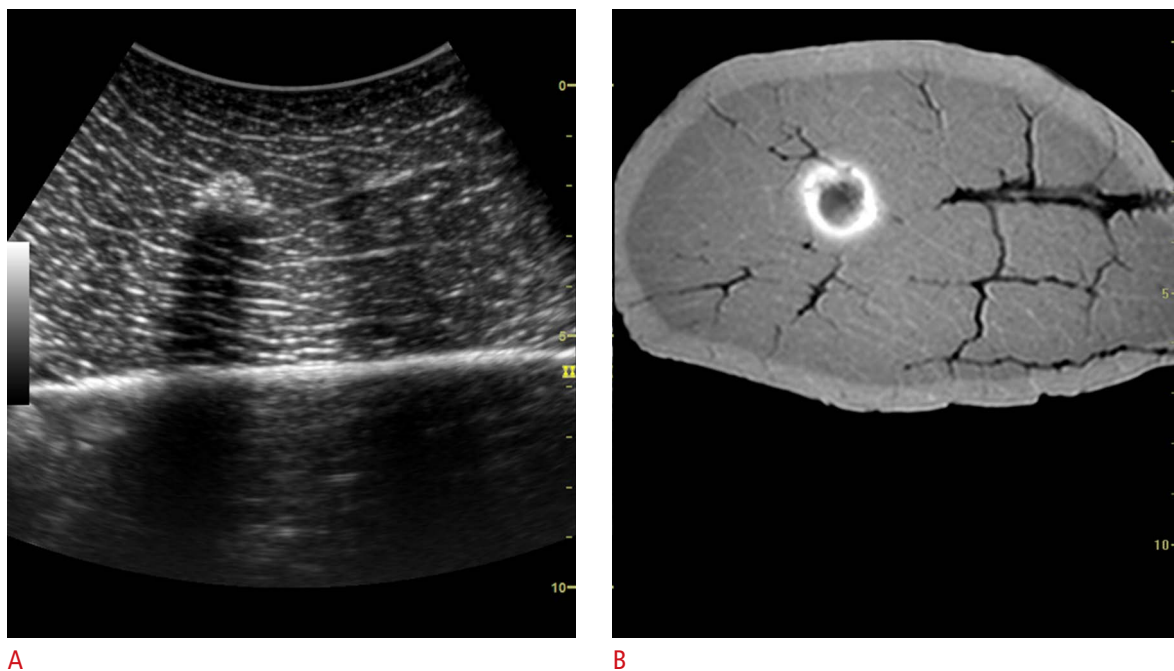


**Fig. 1.** Image fusion before ablation using ultrasonography and magnetic resonance imaging.

A, B. A chickpea was inserted into the rump meat, and ultrasonography (A) and magnetic resonance images (B) were captured before inserting an electrode.

signal intensity different from the surrounding meat on MR images. Twelve chickpeas, about 1.0 cm in diameter, were inserted into 12 blocks of bovine rump meat measuring 10×5×5 cm<sup>3</sup> to create experimental models.

**Imaging**

MR imaging was performed on a 1.5-T MR scanner (Achieva, Philips Healthcare, Best, Netherlands) using a head receiver coil. Axial T1-weighted spin-echo images (TR/TE, 500/10; section thickness, 4 mm) were obtained for four experimental models before and after RF ablation to use as the reference images of fusion imaging and to assess the results of ablation, respectively. The chickpeas were seen as low-signal-intensity nodules with a high signal intensity rim on T1-weighted MR images (Fig. 1A). Three-dimensional US images were acquired before and after RF ablation for all experimental models using a US scanner (Logiq E9, GE Healthcare, Waukesha, WI, USA) and freehand scanning with a transducer that had positioning sensors mounted on it. Three-dimensional US images were obtained with an electrode placed in the experimental model to avoid distortion of the configuration of the models during placement, which can lead to misregistration in image fusion. However, electrode placement was not done before MR imaging due to metallic artifacts. The chickpeas were visualized as hyperechoic nodules on US images (Fig. 1B).

Two types of image fusion were conducted: real-time US with MR and real-time US with 3D US. As the pieces of bovine rump meat did not have any landmarks such as vessels, manual adjustment

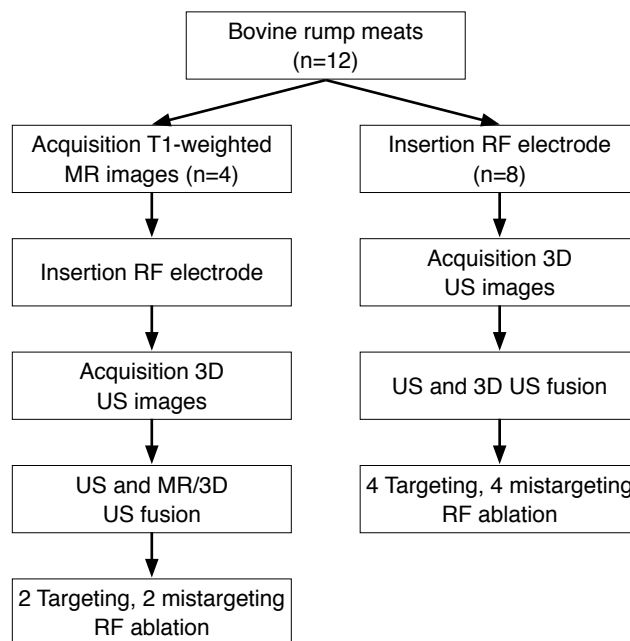


**Fig. 2.** Flow chart of the study population. MR, magnetic resonance; RF, radiofrequency; 3D, 3-dimensional; US, ultrasonography.

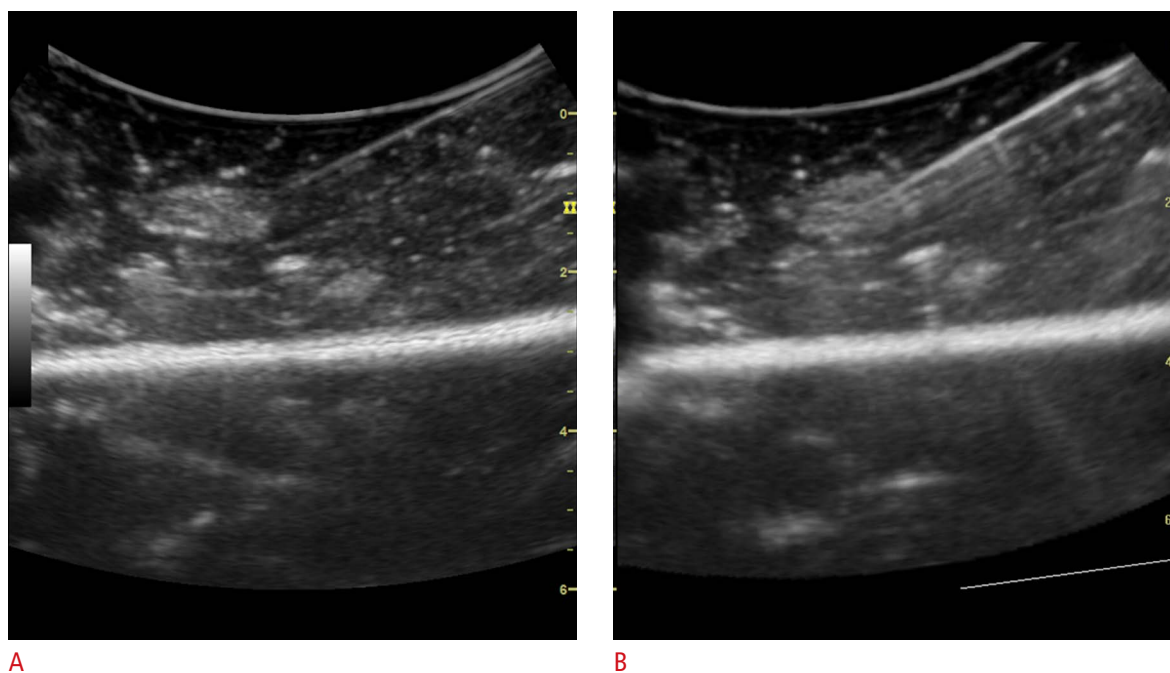


**Fig. 3.** Image fusion before ablation using ultrasonography (US) and 3-dimensional (3D) US. A, B. A chickpea and an electrode were inserted into the rump beef, and US (A) and 3D US (B) images were captured before the chickpea was ablated.

was required, and the tumor substitutes were used as landmarks for image fusion. Four models were prepared for the fusion of real-time US with MR images, whereas the other eight models were used for image fusion of real-time US with 3D US (Fig. 2). The US monitor was configured to display both the real-time US and pre-acquired 3D US or MR images side-by-side. Sensors tracked the position of the transducer, and the split-screen showed the same image planes on the monitor, following the position of the US transducer (Figs. 1, 3).

### RF Ablation

A single radiologist (with more than 15 years of experience in RF ablation) performed the RF ablation procedures in this study. A 17-gauge internally-cooled electrode (Proteus, STARmed, Goyang, Korea) and a 200-W multi-channel RF generator with an impedance-controlled pulsed current (VIVA RF system, STARmed) were used for all ablations. A ground pad was attached to each meat block, which was anchored on a plastic water tank filled with normal saline (Fig. 4). An electrode with a 0.5- or 1-cm active tip was inserted into each meat block under fusion imaging guidance. In six models, the electrode was placed directly in the center of the echogenic tumor substitute, while it was placed outside of the substitute in the

remaining six models. The distance between the off-target electrode and the substitute varied in the six off-target models. RF ablation was done for 2 to 3 minutes with incremental increases in power

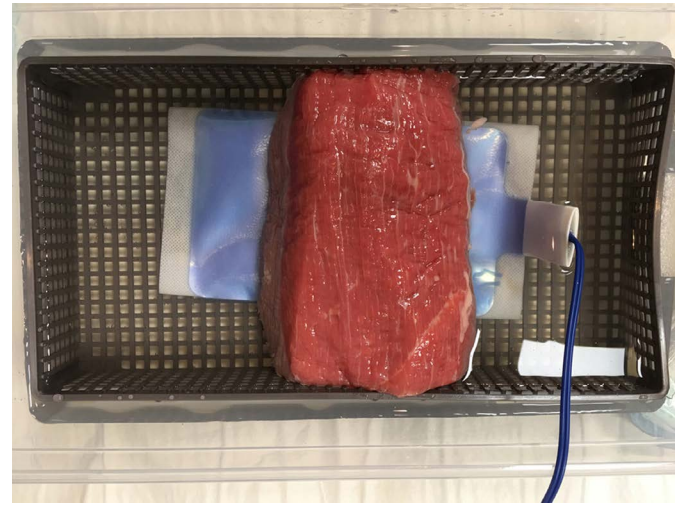


**Fig. 4.** Model used in this study. A piece of bovine rump meat with an attached ground pad was placed in a plastic water tank filled with normal saline. The ground pad was linked to a radiofrequency ablation generator.

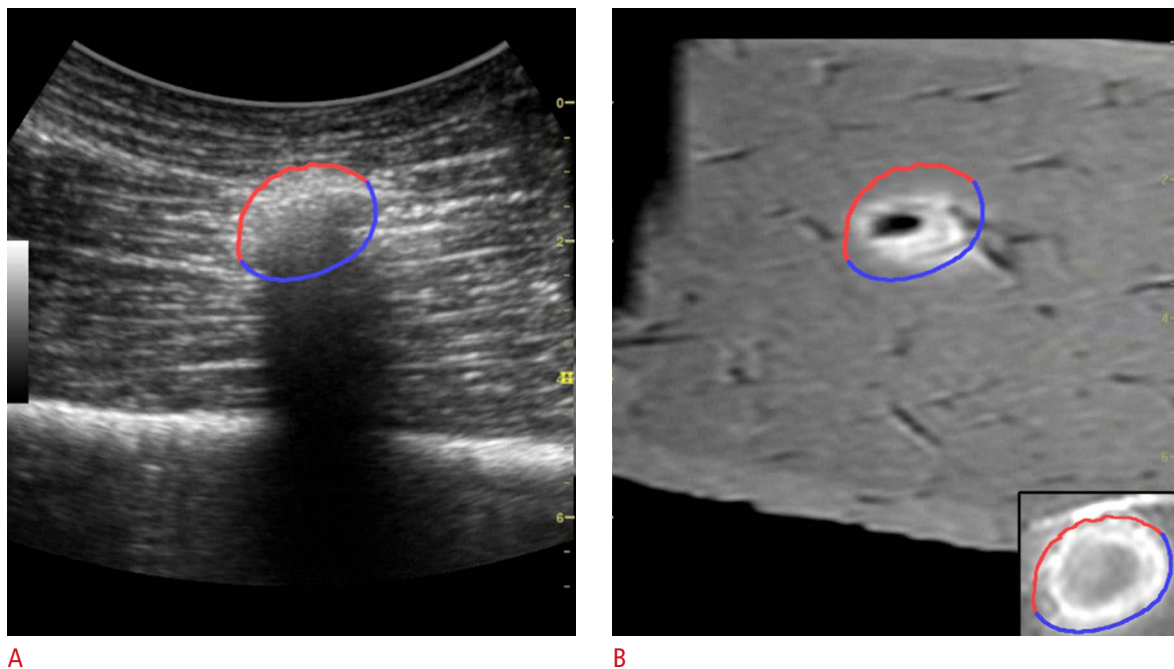


**Fig. 5.** The anterior margin and expected posterior margin of the ablation zone after ablation on ultrasonography (US) and magnetic resonance (MR) images.

**A.** After ablation, the contour of the ablation zone was extracted from the US images. The red contour is the anterior margin and the blue contour is the expected posterior margin. **B.** To evaluate whether the ablation covered the chickpea entirely, the same contour was drawn on the pre-acquired MR image. After ablation, the anterior margin and expected posterior ablative margin were also drawn on the post-ablation MR image (inset in **B**).

until the maximum wattage was reached.

### Estimation of the Ablative Margin

To extract the margin from the hyperechoic zone created during RF ablation, the edge-aware active contour model [21] in the OpenCV v2.4.13 library (<https://opencv.org>) was used. The echogenic zone and surrounding tissue on the real-time US images were classified as the foreground and background, respectively. The contour of the echogenic zone was automatically extracted from the region of interest drawn manually immediately after the ablation procedure. The extracted contour was divided into two areas: the upper side was defined as the anterior margin, while the lower side was defined as the posterior margin. As the shape of the echogenic zone created during ablation is ellipsoidal, and half of the ablation zone margin can be considered the anterior margin, with the other half being the posterior margin, the posterior margin could be estimated from the extracted anterior margin. Because the anterior margin and posterior margin are mirror images, the posterior margin consists of points that are symmetric to the points of the anterior margin. The anterior margin and the expected posterior margin were drawn on the real-time US images and the reference 3D US images or MR images (Figs. 5, 6). Since the anterior margin was correctly determined on the US images, the posterior margin was estimated

correctly. The anterior and posterior margin were overlapped onto an MR image or a 3D US image, and the extent to which the posterior margin covered the tumor was evaluated.

### Evaluation of the Experimental Specimens and Imaging

The experimental specimens were sectioned parallel to the long axis of electrode insertion. Photographs of the sectioned specimens were taken to compare with the 3D US and MR images. The accuracy of the extracted contours from the 12 US fusion videos of real-time US with 3D US or MR images were evaluated by comparing them with the post-ablation MR images using a 3-point scale: 1 (poor), 2 (moderate), and 3 (good). The accuracy was graded as "good" if the entire margin was sufficiently extracted. A "moderate" classification was assigned if the ablation zone was found but the margin was not sufficiently extracted. "Poor" meant that the ablation zone was not found. Post-ablation 3D US and MR images were compared with sectioned specimens to qualitatively evaluate the ablation zone using a 3-point scale: 1 (poor), 2 (moderate), and 3 (good). A score of "good" was assigned if the entire margins of the images and sectioned specimens were coterminous. A "moderate" classification was given if the ablation zones were similar. If the ablation zones were incongruent, the evaluation was "poor." Nicotinamide adenine dinucleotide (NADH) staining of the sectioned specimens

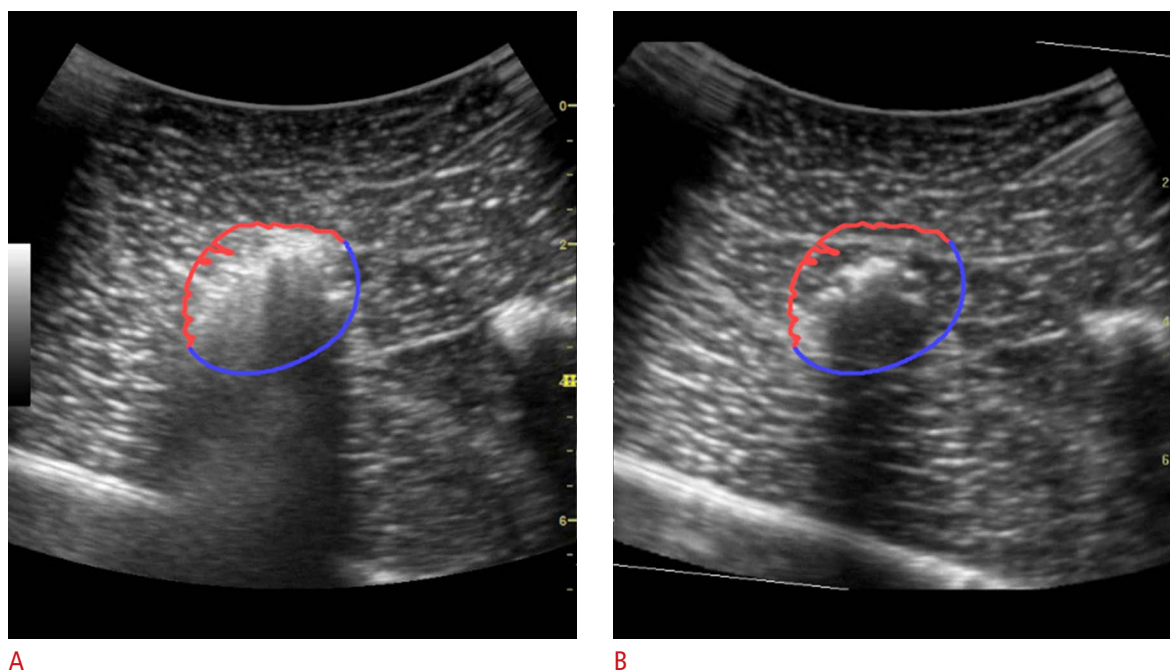


**Fig. 6.** The anterior margin and expected posterior margin of the ablation zone using ultrasonography (US) and 3-dimensional (3D) US. **A.** After ablation, a contour was extracted from the US images. The red contour is the anterior margin and the blue contour is the expected posterior margin. **B.** To evaluate whether the ablation covered the chickpea entirely, the same contour was drawn on the pre-acquired 3D US image.

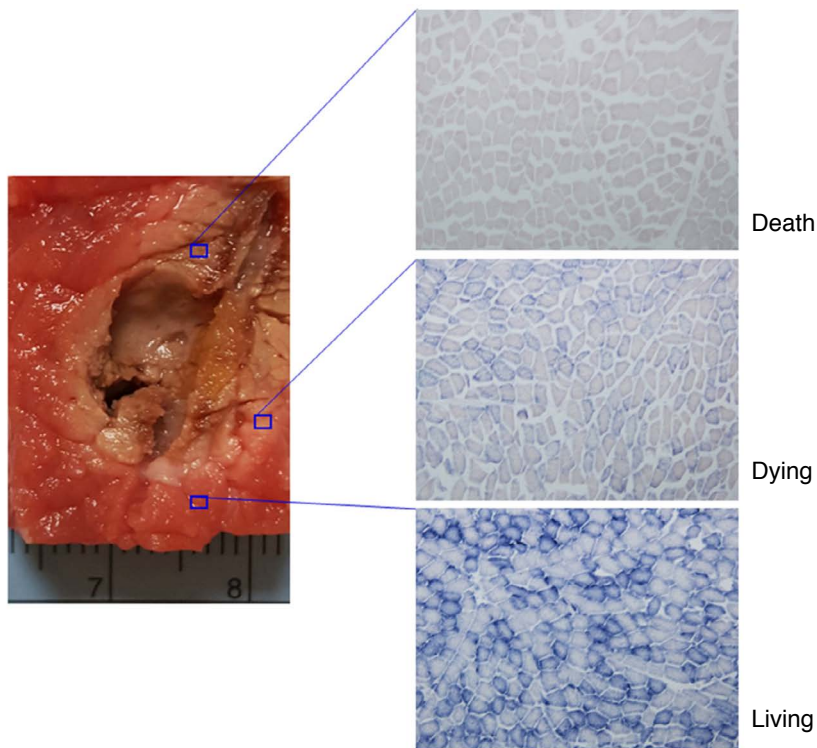


**Fig. 7.** Histopathologic analysis using nicotinamide adenine dinucleotide (NADH). Correlation of cell changes after radiofrequency ablation is shown between the gross images and histopathologic images. After ablation, the bovine rump beef was cut along the electrode path. NADH was used for staining and photographs were taken at  $\times 100$  magnification. There were three categories of cell changes: living, dying, and dead. These cell changes correlated well with the ablation zone.

was performed to evaluate cell viability, and the specimens were classified as necrotic, mixed, or viable. The color of the ablation zone was brown (Fig. 7, upper right), and the area of dying cells was pink (Fig. 7, middle right). The extent of the brown areas in the histopathologic results was practically the same in all specimens.

## Results

The extracted contours of the ablation zones from the 12 real-time US and 3D US fusion videos coincided visually with the sectioned specimens. The meat blocks were distorted by the insertion of an RF electrode, so the real-time US images were different from pre-ablation MR images. Non-rigid registration was therefore used, which eventually caused misregistration. However, additional registration was performed and the tumor substitute in the meat blocks and ablation zone could be identified in real time. Meanwhile, image distortion did not occur to a significant extent when 3D US was used for image fusion, compared with when MR was used.

In the comparison of the real-time US/3D US fusion images with the sectioned specimens, the scores were good in eight and moderate in four. In the comparison of post-ablation MR images with the sectioned specimens, the scores were good in seven and moderate in five. In the comparison with the NADH and histopathologic results, the scores were good in 10 specimens and

moderate in two.

## Discussion

The results of our pilot study indicate that applying an active contour configuration model is a feasible way of predicting the posterior margin of the ablation zone. In the pilot experiment, we verified that bovine livers were not suitable for our study. Explanted livers were not used for the experimental model, as such livers contain air shadows within the portal veins, hepatic vessels and bile ducts, resulting in many types of US artifacts, which are not ideal for experiments. In a pilot study to find an optimal model to simulate small hepatocellular carcinoma, porcine loin cube blocks, black beans, white butter beans, and chickpeas were tested. They were inserted into the bovine rump meat, and T1-weighted MR images and US images were taken. The porcine loin cube block had a similar signal intensity to the meat on MR images and was therefore unsuitable. The black beans and white butter beans were hard to distinguish on MR images and had long shapes, making them unsuitable as tumor substitutes.

RF ablation is widely used to treat hepatic tumors smaller than 3 cm. Its popularity is increasing because it has minimal side effects and is associated with low recurrence rates. In addition, MR fusion imaging can help place an electrode more accurately into

a tumor [22]. Meanwhile, when 3D US fusion is used with real-time US, operators can easily understand 3D information such as the geometry and location of electrodes and anatomical structures, which facilitates repositioning the electrodes if necessary [23]. Positioning sensors are used for US image-guided interventional procedures with reference data sets such as MR or CT images to correctly and rapidly place an electrode in a tumor. Three-dimensional US fusion imaging is a more accurate technique than US MR fusion imaging for placing an electrode where the operator wants. Fusion imaging is especially beneficial for showing and tracking the same image plane.

After ablation has begun, a hyperechoic area begins to be created. During ablation, the tumors and the inserted electrode are inconspicuous, and the posterior margin is also invisible, as it is obscured by the created hyperechoic area.

After ablation, additional treatment is conducted if ablation is inadequate. To reduce patients' hospital stay, expenses, and suffering caused from re-treatment, an accurate assessment during ablation is important to ensure that a sufficient ablative margin has been achieved. Therefore, it is clinically important to accurately estimate the ablation zone during treatment in order to prevent the problems that are caused by re-treatment.

If the extent of the hyperechoic zone created by ablation is 5 mm larger than the tumor, it can be estimated that it has been treated sufficiently. However, it is difficult to correctly distinguish the posterior ablative margin on US due to the posterior dirty shadow from the transient hyperechoic zone. Therefore, the assessment tool that we propose may help overcome this limitation of US imaging in evaluating the margin of ablation zones. The ablation assessment tool estimates the posterior ablative margin and evaluates whether the margin sufficiently covers the tumor.

The expected posterior margin using an active contour model was overlaid onto the pre-ablation MR or 3D US images. This method was more useful than other methods, such as planning before ablation and drawing the ablative margin. This method used in our study was very effective for recognizing the posterior ablative margin and evaluating whether the ablative margin covered the tumor.

This study had a few limitations. First, the results may seem to be subjective because they were assessed by a physician through a visual evaluation rather than by an objective imaging tool program. However, visual evaluation may be more practical in clinical settings. Second, as this study used meat samples, the software used in this study may not be as applicable when used in actual clinical practice where free breathing is allowed. Third, the number of experimental models in this study was small. More preclinical studies are required to determine whether this software can be applied in clinical studies.

In conclusion, we have shown the feasibility of an active contour configuration model for estimating the posterior ablative margin on US, fused with 3D US or MR images, for RF ablation.

ORCID: Junkyo Lee: <http://orcid.org/0000-0001-9700-6377>; Min Woo Lee: <http://orcid.org/0000-0001-9048-9011>; Dongil Choi: <http://orcid.org/0000-0001-7176-8808>; Dong Ik Cha: <http://orcid.org/0000-0002-9116-3803>; Sunyoung Lee: <http://orcid.org/0000-0003-1416-3866>; Tae Wook Kang: <http://orcid.org/0000-0002-8991-6407>; Jehoon Yang: <http://orcid.org/0000-0002-5808-9998>; Jaemoon Jo: <http://orcid.org/0000-0003-3096-0558>; Won-Chul Bang: <http://orcid.org/0000-0003-3175-7551>; Jongsik Kim: <http://orcid.org/0000-0002-6520-427X>; Dongkuk Shin: <http://orcid.org/0000-0001-6565-672X>

#### \*Author affiliations

<sup>1</sup>Department of Health Sciences and Technology, Samsung Advanced Institute for Health Sciences and Technology, Sungkyunkwan University, Seoul; <sup>2</sup>Medical Imaging R&D Group, SAMSUNG MEDISON Co., Ltd., Seoul; <sup>3</sup>Department of Radiology and Center for Imaging Science, Samsung Medical Center, Sungkyunkwan University School of Medicine, Seoul; <sup>4</sup>Laboratory Animal Research Center, Samsung Biomedical Research Institute, Seoul; <sup>5</sup>Advanced R&D Team, Samsung Electronics, Suwon; <sup>6</sup>Medical Imaging R&D Group, Samsung Electronics, Suwon, Korea

#### Conflict of Interest

No potential conflict of interest relevant to this article was reported.

## References

1. Livraghi T, Goldberg SN, Lazzaroni S, Meloni F, Solbiati L, Gazelle GS. Small hepatocellular carcinoma: treatment with radio-frequency ablation versus ethanol injection. *Radiology* 1999;210:655-661.
2. Sutherland LM, Williams JA, Padbury RT, Gotley DC, Stokes B, Maddern GJ. Radiofrequency ablation of liver tumors: a systematic review. *Arch Surg* 2006;141:181-190.
3. Rossi S, Buscarini E, Garbagnati F, Di Stasi M, Quaretti P, Rago M, et al. Percutaneous treatment of small hepatic tumors by an expandable RF needle electrode. *AJR Am J Roentgenol* 1998;170:1015-1022.
4. Buscarini L, Buscarini E, Di Stasi M, Vallisa D, Quaretti P, Rocca A. Percutaneous radiofrequency ablation of small hepatocellular carcinoma: long-term results. *Eur Radiol* 2001;11:914-921.
5. Wood BJ, Locklin JK, Viswanathan A, Kruecker J, Haemmerich D, Cebal J, et al. Technologies for guidance of radiofrequency ablation in the multimodality interventional suite of the future. *J Vasc Interv Radiol* 2007;18(1 Pt 1):9-24.
6. Ewertsen C, Saftoiu A, Gruionu LG, Karstrup S, Nielsen MB. Real-time image fusion involving diagnostic ultrasound. *AJR Am J Roentgenol* 2013;200:W249-W255.

7. Machi J, Uchida S, Sumida K, Limm WM, Hundahl SA, Oishi AJ, et al. Ultrasound-guided radiofrequency thermal ablation of liver tumors: percutaneous, laparoscopic, and open surgical approaches. *J Gastrointest Surg* 2001;5:477-489.
8. Kang TW, Lee MW, Choi SH, Rhim H, Lim S, Song KD, et al. A novel electrode with electromagnetic tip tracking in ultrasonography-guided radiofrequency ablation: a phantom, ex vivo, and in vivo experimental study. *Invest Radiol* 2015;50:81-87.
9. Lee MW, Rhim H, Cha DI, Kim YJ, Choi D, Kim YS, et al. Percutaneous radiofrequency ablation of hepatocellular carcinoma: fusion imaging guidance for management of lesions with poor conspicuity at conventional sonography. *AJR Am J Roentgenol* 2012;198:1438-1444.
10. Villard C, Soler L, Gangi A. Radiofrequency ablation of hepatic tumors: simulation, planning, and contribution of virtual reality and haptics. *Comput Methods Biomech Biomed Engin* 2005;8:215-227.
11. Stone MJ, Wood BJ. Emerging local ablation techniques. *Semin Intervent Radiol* 2006;23:85-98.
12. Kim YS, Lee WJ, Rhim H, Lim HK, Choi D, Lee JY. The minimal ablative margin of radiofrequency ablation of hepatocellular carcinoma (> 2 and < 5 cm) needed to prevent local tumor progression: 3D quantitative assessment using CT image fusion. *AJR Am J Roentgenol* 2010;195:758-765.
13. Wang XL, Li K, Su ZZ, Huang ZP, Wang P, Zheng RQ. Assessment of radiofrequency ablation margin by MRI-MRI image fusion in hepatocellular carcinoma. *World J Gastroenterol* 2015;21:5345-5351.
14. Solbiati L, Goldberg SN, Ierace T, Dellanoce M, Livraghi T, Gazelle GS. Radio-frequency ablation of hepatic metastases: postprocedural assessment with a US microbubble contrast agent: early experience. *Radiology* 1999;211:643-649.
15. Tokunaga S, Koda M, Matono T, Sugihara T, Nagahara T, Ueki M, et al. Assessment of ablative margin by MRI with ferucarbotran in radiofrequency ablation for liver cancer: comparison with enhanced CT. *Br J Radiol* 2012;85:745-752.
16. Okuwaki Y, Nakazawa T, Shibuya A, Ono K, Hidaka H, Watanabe M, et al. Intrahepatic distant recurrence after radiofrequency ablation for a single small hepatocellular carcinoma: risk factors and patterns. *J Gastroenterol* 2008;43:71-78.
17. Nakazawa T, Kokubu S, Shibuya A, Ono K, Watanabe M, Hidaka H, et al. Radiofrequency ablation of hepatocellular carcinoma: correlation between local tumor progression after ablation and ablative margin. *AJR Am J Roentgenol* 2007;188:480-488.
18. Rossi S, Fornari F, Buscarini L. Percutaneous ultrasound-guided radiofrequency electrocautery for the treatment of small hepatocellular carcinoma. *J Interv Radiol* 1993;8:97-103.
19. Fornage BD, Sneige N, Ross MI, Mirza AN, Kuerer HM, Edeiken BS, et al. Small (< or = 2-cm) breast cancer treated with US-guided radiofrequency ablation: feasibility study. *Radiology* 2004;231:215-224.
20. McGhana JP, Dodd GD 3rd. Radiofrequency ablation of the liver: current status. *AJR Am J Roentgenol* 2001;176:3-16.
21. Kass M, Witkin A, Terzopoulos D. Snakes: active contour models. *Int J Comput Vis* 1988;1:321-331.
22. Zaidi H, Montandon ML, Alavi A. The clinical role of fusion imaging using PET, CT, and MR imaging. *PET Clin* 2008;3:275-291.
23. Lee MW. Fusion imaging of real-time ultrasonography with CT or MRI for hepatic intervention. *Ultrasonography* 2014;33:227-239.